Ref. Ares(2026)9980182 - 23/10/2026

BE-LIGHT

Improving biomedical diagnosis through light–based technologies and machine learning

Doctoral Networks (MSCA-DN)

HORIZON - MSCA - 2022 - DN

Grant Agreement Nº 101119924

WP1: *Eye diseases and vision*

Deliverable D1.4
TMV System

Raúl Urriza Arpal, NCU

Ireneusz Grulkowski, NCU

Date: 08 OCTOBER 2026

Type: DEM — Demonstrator, pilot, prototype.
Dissemination Level: PU-Public

Funded by the European Union

DELIVERABLE IDENTIFICATION SHEET

Document version	Date	Editor	Change(s)
1	21-10-2026	Ireneusz Grulkowski	First version

Grant Agreement Nº	101119924
Call Identifier	HORIZON - MSCA - 2022 – DN
Acronym	BE-LIGHT
Full title	Improving biomedical diagnosis through light-based technologies and machine learning
Project URL	http://www.belightproject.eu/

Deliverable Nº and Name	D1.4 TMV system
Work Package	WP1 Eye diseases and vision
Lead Beneficiary	NCU
Type	DEM – Demonstrator, pilot, prototype.
Dissemination Level	PU-Public
Due date	Month 24

Authors (Partner)	Raúl Urriza Arpal, NCU Ireneusz Grulkowski, NCU			
Responsible Author	Raúl Urriza Arpal		**Email**	raul.urriza@umk.pl
	Partner	NCU	**Phone**	+48/56/611-32-97

Abstract (for dissemination)	This deliverable reports the development and experimental validation of a tomographic micro-vibrometry (TMV) system combining high-speed swept-source optical coherence tomography (SS-OCT) with non-contact acoustic micro-tapping for biomechanical characterization of soft tissues. The developed system employs a 1310 nm wavelength-swept laser operating at 200 kHz and an air-coupled, cylindrically focused ultrasound transducer to generate localized mechanical excitation and monitor the resulting elastic wave propagation. Phase-sensitive OCT detection and a dedicated BM-mode acquisition protocol enable depth-resolved measurements of transient tissue displacements and reconstruction of spatiotemporal wave propagation maps. Experimental characterization demonstrated an axial imaging range of 8 mm, an axial resolution of 8.6 µm in air, a detection sensitivity of 99.1 dB, and a phase stability of approximately 5 mrad. The performance of the integrated platform was evaluated using tissue-mimicking gelatin phantoms with different mechanical properties. Elastic wave propagation was successfully visualized, with measured velocities of 0.51 m/s and 0.98 m/s in 2% and 5% gelatin phantoms, respectively. These results demonstrate the feasibility of non-contact, phase-sensitive OCT measurements for detecting differences in tissue mechanical response and establish a

	foundation for further development of quantitative elastography methods, particularly for corneal biomechanics and ophthalmic applications.
Keywords	Optical Coherence Elastography, Cornea, Ultrasound

Table of Contents

DELIVERABLE IDENTIFICATION SHEET 2
EXECUTIVE SUMMARY 4
INTRODUCTION 4
1 OPTICAL PROBING OF SAMPLE DISPLACEMENT FOR MECHANICAL CHARACTERIZATION 5
1.1 Design of OCT instrument 5
1.2 Phase-sensitive detection of displacement 7
1.3 Methodology of characterization of optical system 7
2 MECHANICAL STIMULATION 9
2.1 Geometry 9
2.2 Electrical excitation of the transducer 10
3 SYSTEM INTEGRATION 11
3.1 Hardware integration 11
3.2 Synchronization 12
3.3 Data acquisition protocol 13
4 RESULTS 14
4.1 OCE system with air-borne ultrasound stimulation 14
4.2 Performance of the system 17
4.3 Visualization of shear wave propagation 19
5 SUMMARY & CONLUSIONS 21
REFERENCES 22

EXECUTIVE SUMMARY

In this deliverable, we present the development and experimental validation of a tomographic micro-vibrometry (TMV) system that integrates high-speed swept-source optical coherence tomography (SS-OCT) with non-contact acoustic micro-tapping for the biomechanical characterization of soft tissues. Over the past two years, we have shown that the system enables depth-resolved measurement of transient tissue displacements and the reconstruction of spatiotemporal maps of wave propagation. The system is based on a 1310 nm wavelength-swept laser running at 200 kHz, combined with an air-coupled, cylindrically focused ultrasound transducer that delivers localized mechanical excitation, while the resulting elastic wave propagation is monitored.

The integrated platform was tested on tissue-mimicking gelatin phantoms with different mechanical properties. Elastic wave propagation was clearly visualized, and wave velocities of 0.51 m/s and 0.98 m/s were measured in the 2% and 5% gelatin phantoms, respectively. These findings confirm that non-contact, phase-sensitive OCT measurements can detect differences in the mechanical response of tissue, and they provide a basis for the further development of quantitative elastography methods, especially for corneal biomechanics and ophthalmic applications.

INTRODUCTION

The assessment of tissue biomechanical properties is increasingly recognized as an important approach for understanding tissue physiology, detecting pathological alterations, and developing novel diagnostic biomarkers [1]. Changes in tissue stiffness, elasticity, and viscoelastic behavior often accompany structural remodeling, aging, and disease progression [2-4]. However, conventional methods for mechanical characterization frequently require direct contact with the sample or are unsuitable for high-resolution, spatially resolved measurements. Optical coherence elastography (OCE), combining the high spatial resolution and sensitivity of optical coherence tomography (OCT) with controlled mechanical excitation, offers a promising approach for quantitative, minimally invasive assessment of tissue biomechanics [5].

Within the BE-LIGHT project, a swept-source optical coherence tomography (SS-OCT) system integrated with focused ultrasound micro-tapping has been developed to investigate the propagation of mechanically induced elastic waves in biological tissues. Focused ultrasound provides localized, transient mechanical excitation, generating shear-dominated waves that propagate through the tissue. The SS-OCT system enables highly sensitive detection of the resulting tissue displacements and tracking of wave propagation with high spatial and temporal resolution. Analysis of wave propagation characteristics, including velocity, provides information about the underlying mechanical properties of the investigated tissue [6]. The instrument can be considered as an optical vibrometer.

This deliverable presents the developed experimental platform, including the optical imaging subsystem, ultrasound excitation module, synchronization and acquisition procedures, and data processing methods for monitoring shear wave propagation. The system establishes a technological foundation for investigating tissue biomechanics and developing quantitative imaging biomarkers with potential applications in biomedical diagnostics and disease monitoring. The study of mechanical properties of tissues is an area of broad interest in medicine.

1 Optical Probing of Sample Displacement for Mechanical Characterization

The reaction of the sample to mechanical excitation was probed with optical interferometry set-up using SS-OCT technology. The concept relies on the generation of localized mechanical perturbations using a focused ultrasound transducer and the subsequent detection of propagating elastic waves by phase-sensitive OCT. The SS-OCT subsystem provides depth-resolved structural imaging while simultaneously measuring nanometer-scale tissue displacements through analysis of the phase variations of the OCT signal. By recording the temporal evolution of sample motion at different spatial locations, the system enables visualization and quantitative characterization of elastic wave propagation. The acquired spatiotemporal displacement data can be analyzed to determine wave propagation parameters, including group and phase velocities, frequency-dependent dispersion, and attenuation. Combined with appropriate mechanical models, these parameters can be used to estimate tissue mechanical properties, such as shear modulus, elasticity, and viscoelasticity.

The technology used in this deliverable offers several distinct advantages as a detection modality for elastographic measurements. Its combination of high spatial resolution, **depth-resolved imaging**, and **exceptional sensitivity to microscopic displacements** makes OCT particularly suitable for investigating the mechanical response of tissues to external excitation. Unlike conventional elastography [7], OCT enables micrometer-scale visualization of tissue microstructure while phase-sensitive detection provides sensitivity to tissue displacements at the nanometer scale [5]. This capability is particularly important when investigating small-amplitude elastic waves generated by non-contact mechanical stimulation, such as focused ultrasound micro-tapping. Furthermore, the **high acquisition rates** achievable with SS-OCT facilitate time-resolved monitoring of elastic wave propagation, allowing the extraction of wave velocity, attenuation, and frequency-dependent dispersion characteristics. Another important advantage is the **ability to correlate biomechanical measurements directly with the structural organization of the tissue**, enabling the identification of local mechanical heterogeneities and their relationship to specific morphological features. The **non-invasive and non-contact nature of OCT**, together with its compatibility with repeated measurements, makes it particularly attractive for studying delicate biological tissues and monitoring biomechanical changes over time.

1.1 Design of OCT instrument

The optical TMV system developed for elastographic measurements was based on a fiber-optic SS-OCT configuration (Fig. 1). The instrument used a wavelength-swept vertical-cavity surface emitting laser (SL132121; Thorlabs Inc.) operating at an A-scan rate of 200 kHz, with a central wavelength of 1310 nm and a spectral tuning bandwidth of approximately 130 nm.

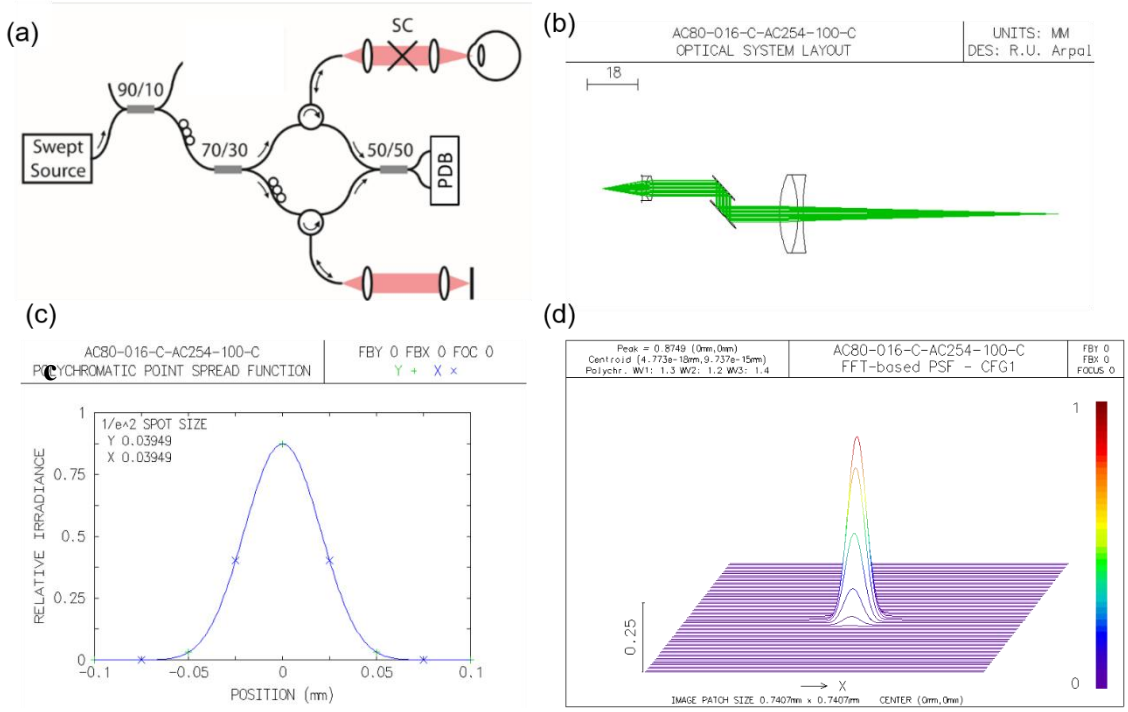

Figure 1. (a) Schematic of the TMV system (b) OSLO ray-trace layout of the sample arm. (c) Profile of the on-axis polychromatic PSF: 1/e² radius 39.5 µm (FWHM ≈ 46 µm). (d) FFT-based PSF. Strehl ratio = 0.87, the system is diffraction-limited on axis.

Light emitted by the swept laser is initially divided using a 90/10 fiber coupler, with a fraction of the optical power directed towards an auxiliary Mach–Zehnder interferometer (MZI), which can serve as a reference for wavelength-sweep calibration. The remaining light is delivered to the main OCT interferometer, where a 70/30 fiber coupler distributes the optical power between the reference and sample arms. Both interferometer arms incorporate fiber-optic circulators, which separate the incident and backscattered light and direct the returning optical signals towards the detection unit. Fiber polarization controllers are included to optimize the interference signal contrast by matching the polarization states of light returning from both arms.

In the reference arm, the light is collimated and focused onto a stationary mirror, whereas the sample arm incorporates a beam-scanning head consisting of two galvanometric mirrors (XY) and focusing optics (f = 100 mm). The scanning optics allow the probing beam to be positioned at selected locations on the tissue surface, facilitating both conventional cross-sectional imaging and spatially resolved displacement measurements.

The optical signals returning from the sample and reference arms are recombined using a 50/50 fiber coupler, and the resulting interference signals are detected by a high-speed photodetection unit (balanced photodetector PDB480C-AC, 1.6 GHz, InGaAs, Thorlabs). The interferometric signals were digitized using a 12-bit digitizer board (ATS9373, Alazar Technologies Inc.). A sample illumination power was 4.38 mW. The acquisition card operated in a clocked mode since the laser a k-clock signal generated by the integrated Mach-Zehnder interferometer. Therefore, the acquired interference signals did not require any numerical resampling into the wavenumber domain and Fourier transformation to reconstruct the depth-resolved OCT signal.

1.2 Phase-sensitive detection of displacement

Phase-sensitive OCT enables highly sensitive measurements of tissue displacement by exploiting the phase information encoded in the interferometric signal. In conventional OCT imaging, the amplitude of the reconstructed complex signal is used to visualize the internal microstructure of the sample. However, the phase of the OCT signal contains additional information about the optical path length between the reference arm and scattering structures within the investigated tissue. Consequently, even very small axial movements of tissue scatterers introduce measurable changes in the phase of the interference signal.

The spectral interference signal is acquired during each wavelength sweep of the laser source. After Fourier transformation, a complex-valued depth-resolved signal is reconstructed. The amplitude of this signal represents the local backscattering properties of the tissue, whereas its argument corresponds to the interferometric phase. By comparing complex OCT signals acquired at consecutive time points, changes in the optical phase can be determined for individual scattering structures located at different depths.

$$\Delta\varphi(z,t) = arg\{A(z,t) \cdot A^*(z,t-\Delta t)\},$$

where: $A(z, t)$ denotes the complex OCT signal at depth z and time t, A^* represents its complex conjugate, and Δt is the time interval between successive measurements (A-scans).

Assuming that the observed phase variations originate from the axial displacement of tissue scatterers, the corresponding displacement along the OCT beam can be calculated using:

$$\Delta z(z,t) = \frac{\lambda_0 \Delta\varphi(z,t)}{4\pi n},$$

where λ_0 is the central wavelength of the light source and n is the refractive index of the investigated medium. In the developed SS-OCT system operating at approximately 1300 nm, this relationship enables the detection of very small axial displacements, reaching nanometer-range sensitivity, depending on the phase stability and signal-to-noise ratio of the instrument. The available displacement range (without observation of phase wrapping) is given by:

$$\Delta z_{max}(z,t) = \pm\frac{\lambda_0}{4n}.$$

1.3 Methodology of characterization of optical system

The performance of the developed SS-OCT system was characterized using standard experimental procedures commonly employed for Fourier-domain OCT systems. The characterization included measurements of: the axial imaging range, sensitivity roll-off, axial resolution, detection sensitivity, and phase stability. These parameters determine the system's capability to provide high-resolution structural imaging and to detect small tissue displacements induced by ultrasound stimulation.

Axial (depth) imaging range and sensitivity roll-off

The axial imaging range and sensitivity roll-off were evaluated by recording the OCT signal reflected from a mirror at different optical path length differences between the

interferometer arms. The position of the mirror signal in the reconstructed A-scan was varied systematically across the available axial imaging range. At each depth, the amplitude of the reflection peak was measured to determine the depth-dependent signal.

The sensitivity roll-off was calculated as the ratio between the OCT signal amplitude measured at a given depth and the maximum signal amplitude obtained near the reference position (OPD = 0). The resulting roll-off curve describes the decrease in OCT signal amplitude as a function of imaging depth. The axial distance at which the signal decreases by 6 dB relative to its maximum value was used to characterize the effective sensitivity range of the system.

Axial resolution

The axial resolution was evaluated experimentally by measuring the axial point spread function (PSF) obtained from a mirror placed in the sample arm. The reflected signal was reconstructed using the standard OCT processing procedure, and the axial intensity distribution around the reflection peak was analyzed. The axial resolution was determined from the full width at half maximum (FWHM) of the reconstructed PSF, expressed in micrometers.

System sensitivity

The detection sensitivity of the SS-OCT system was characterized using a calibrated reflection signal and a known optical attenuation introduced into the sample arm. A mirror was positioned near the focal plane of the sample-arm optics. A calibrated neutral density filter was placed in the optical path to reduce the backreflected power and avoid saturation of the photodetector. The OCT signal was acquired, and the signal-to-noise ratio (SNR) was calculated by comparing the intensity of the reconstructed reflection peak with the background noise level obtained from a signal-free region of the reconstructed depth profile. The system sensitivity was determined by correcting the measured SNR for the known optical attenuation and the reflectance of the calibration sample:

$$Sensitivity\ (dB) = 10log_{10}\left(I_{peak}/\sigma_{noise}\right) - 20log_{10}(T),$$

where I_{peak} is the reconstructed peak intensity, σ_{noise} is the mean background noise intensity, and T is the single-pass power transmission of the attenuation filter.

The sensitivity measurements were conducted under defined illumination conditions, with the optical power incident on the sample measured using an optical power meter. The acquisition parameters and signal-processing conditions were maintained consistently throughout the measurements. The resulting sensitivity was expressed in decibels and represents the minimum sample reflectance that can be detected with an SNR of unity under the specified experimental conditions.

Phase stability and displacement sensitivity

Phase stability is one of the most important parameters of the SS-OCT system when applied to optical coherence elastography. Since tissue displacement is determined from changes in the interferometric phase, random phase fluctuations introduce uncertainty into the measured displacement and establish the noise floor of the elastographic measurement.

The phase stability was evaluated using a stationary mirror positioned in the sample arm of the interferometer. A sequence of consecutive A-scans was acquired at a fixed lateral

position without applying any external mechanical excitation. The phase noise was quantified by calculating the standard deviation of the differential phase signal:

$$\sigma_{\varphi} = StD[\Delta\varphi(t)].$$

The phase noise can be subsequently converted into the equivalent axial displacement noise using:

$$\sigma_{\Delta z} = \frac{\lambda_0}{4\pi n}\sigma_{\varphi},$$

where σ_{φ} is the displacement noise, λ_0 is the central wavelength of the laser, and n is the refractive index of the investigated medium.

2 Mechanical Stimulation

Non-contact excitation is preferred for in vivo measurements, since it avoids discomfort, the need for anaesthesia and the risk of infection or epithelial damage. However, the conventional mechanical stimulation strategies are based on the air puff that induces a large, global deformation [8,9]. Air-coupled ultrasound transducers instead use acoustic radiation force to generate small, localized displacements on the micrometre scale, which are well suited to launching shear waves [10,11].

2.1 Geometry

The mechanical excitation subsystem is based on the acoustic micro-tapping technique originally developed by Ambroziński et al. [10]. This approach employs a specially designed, air-coupled piezoelectric ultrasound transducer to generate localized mechanical perturbations at the surface of the sample without direct physical contact.

The ultrasound excitation module is based on a cylindrically focused piezoelectric transducer (Fig. 2). To improve acoustic energy transmission from the piezoelectric element into air, a matching layer consisting of a porous nylon membrane was attached to the emitting surface using silicone adhesive. This configuration provides efficient generation of focused ultrasonic pulses in air, overcoming the substantial acoustic impedance mismatch between the piezoelectric material and the surrounding medium.

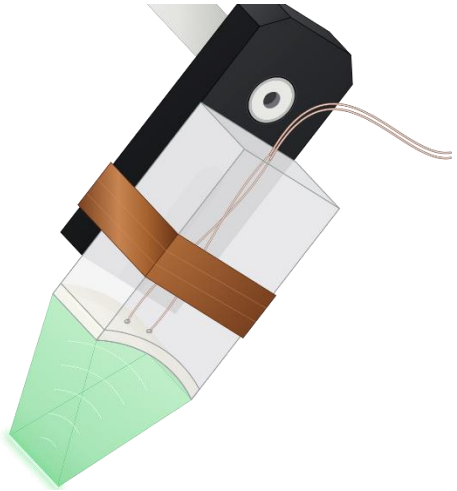

Figure 2. Scheme of the ultrasound transducer.

An important feature of the transducer is its cylindrical focusing geometry. Unlike spherically focused transducers, which generate a relatively small focal spot, the cylindrical element produces an elongated, line-shaped acoustic intensity distribution. When positioned near the sample surface, the acoustic field creates a narrow strip of mechanical excitation extending along the focal line. The focal line is oriented approximately perpendicular to the intended direction of elastic wave propagation, producing nearly planar propagating wavefronts over the investigated region.

2.2 Electrical excitation of the transducer

The piezoelectric transducer was driven using a programmable arbitrary waveform generator (TGA12102, TTi, UK) connected to a high-voltage amplifier (Fig. 3).

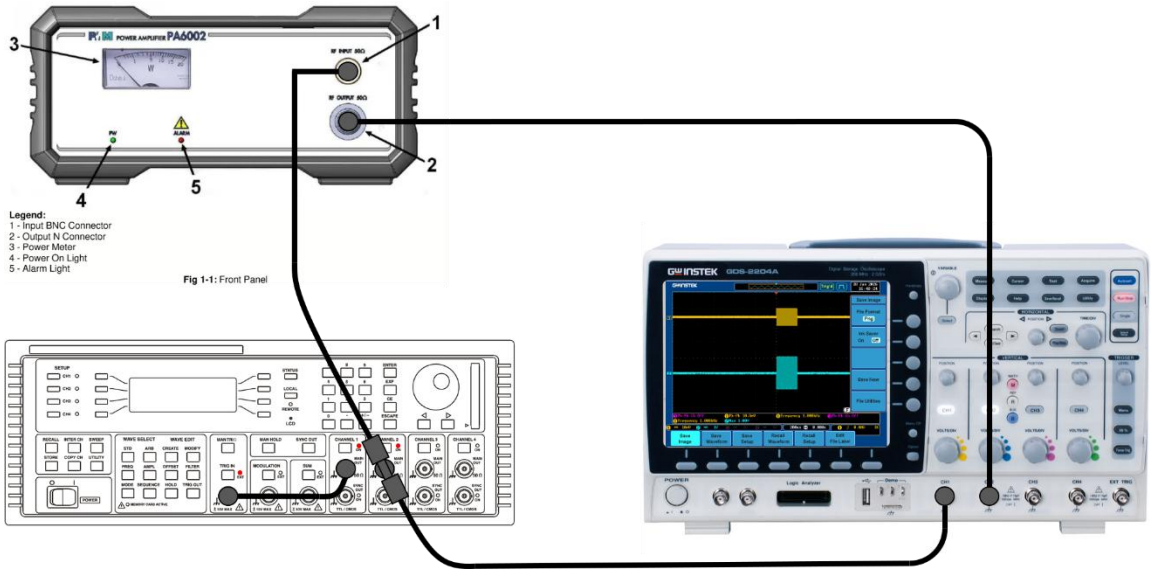

Figure 3. Excitation set-up: signal generator, RF power amplifier (PA6002) and oscilloscope (GDS-2204A).

The waveform generator was configured to produce sinusoidal bursts at a carrier frequency of 1.04 MHz, corresponding to the operating frequency of the ultrasonic transducer. Each excitation burst consisted of 200 sinusoidal cycles, resulting in an excitation duration of approximately 192 µs (Fig. 4). The electrical signal generated at channel CH1 was amplified and subsequently delivered to the piezoelectric transducer to generate a focused ultrasonic field. During experimental measurements, the output amplitude of the waveform generator was adjusted up to 10 Vpp, corresponding to approximately 170 Vpp at the amplifier output. The excitation amplitude was increased gradually to prevent amplifier overload and ensure stable operation of the transducer. An excitation voltage of approximately 200 Vpp was established as the upper operating limit for the transducer. The electrical excitation waveform was monitored using an oscilloscope equipped with a high-voltage-compatible attenuating probe, allowing verification of the burst duration, amplitude, and waveform shape.

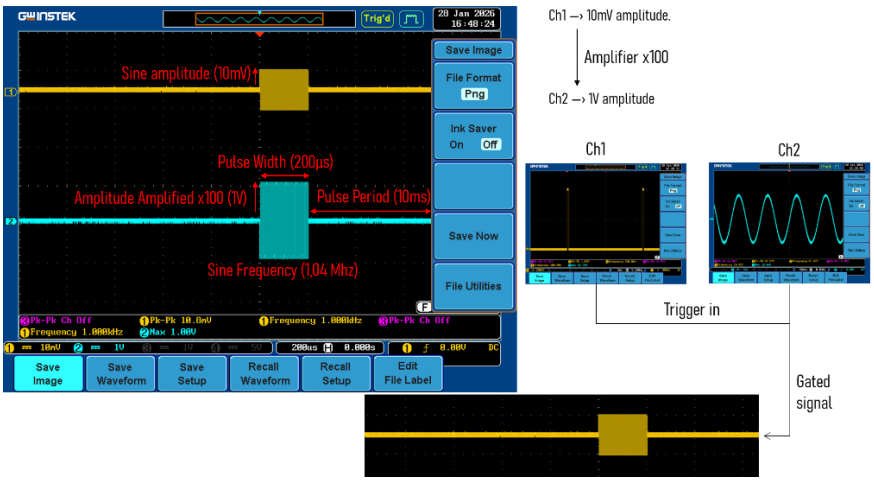

Figure 4. Excitation signal: 1.04 MHz, 200 µs burst each 10ms before and after ×100 amplification.

3 System Integration

3.1 Hardware integration

For elastographic measurements, the phase-sensitive OCT acquisition is synchronized with the focused ultrasound excitation. The ultrasound pulse generates a localized mechanical perturbation, resulting in the propagation of elastic waves through the investigated tissue. Repeated OCT measurements performed at a fixed lateral position (M-mode acquisition) allow the temporal evolution of tissue displacement to be recorded with high temporal resolution. By repeating the excitation and acquisition sequence at multiple lateral positions, the displacement field can be reconstructed as a function of both space and time. This enables visualization of the propagating elastic wavefront and quantitative determination of wave propagation characteristics, including propagation velocity and frequency-dependent dispersion.

The transducer was positioned at an oblique angle relative to the tissue surface normal, approximately 45° in the original configuration, to provide sufficient optical access for the OCT probing beam (Fig. 5). The acoustic focal region was adjusted to coincide with the tissue surface. When a short burst of ultrasound reaches the air–tissue interface, this localized mechanical loading induced small tissue displacements and launches elastic waves that propagate laterally away from the excitation region (shear wave).

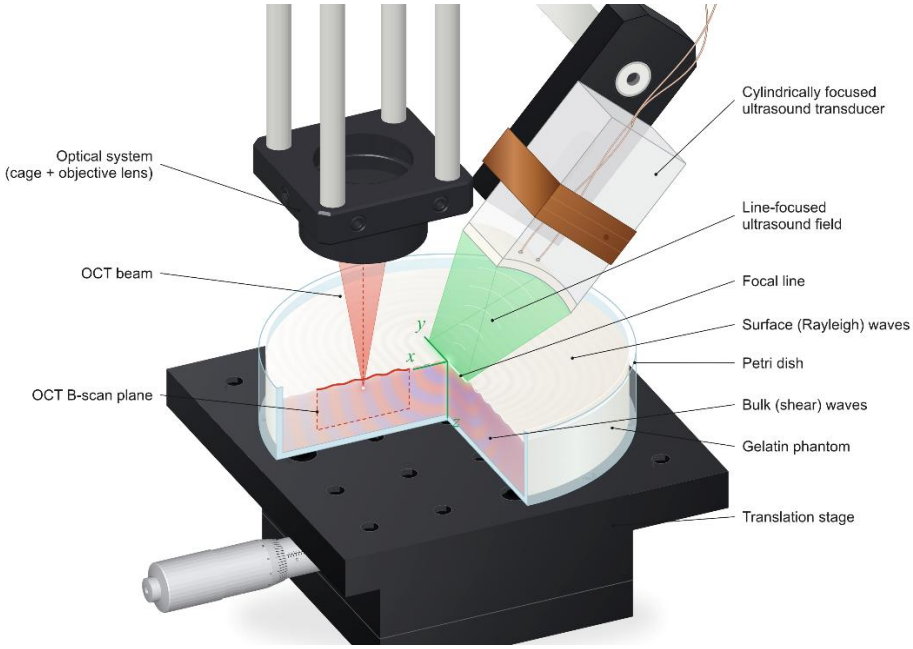

Figure 5. Experimental set-up: the cylindrical transducer generates a line-focused ultrasound stimulating a gelatin phantom, and the induced shear waves are imaged in the OCT B-scan plane.

3.2 Synchronization

To ensure precise temporal synchronization between the ultrasound excitation and OCT acquisition, the waveform generator was operated in externally triggered mode. The synchronization signal was generated by the AlazarTech ATS9373 data acquisition board, with its auxiliary input/output (AUX I/O) to provide an output trigger. This signal was delivered to the external trigger input (TRIG IN) of the waveform generator, initiating a single ultrasound excitation burst for each trigger event. The same synchronization signal was also distributed to the optical scanning subsystem through a National Instruments PCIe-6363 multifunction data acquisition board and BNC-2110 connector block. This configuration ensured a reproducible temporal relationship between the mechanical excitation and OCT measurements, enabling phase-sensitive detection of tissue displacements and reconstruction of the spatiotemporal propagation of elastic waves (Fig. 6).

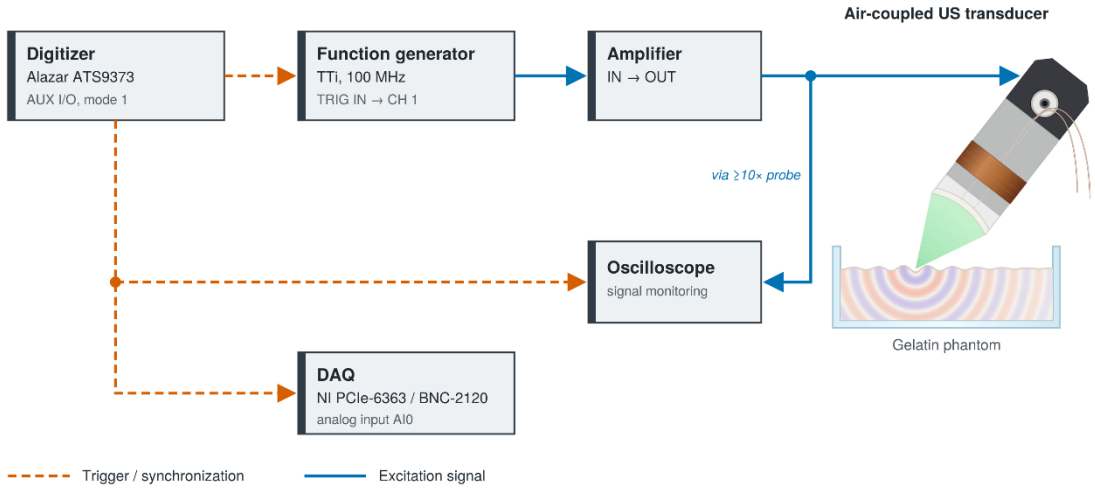

Figure 6. Synchronization of the acquisition sub-system with ultrasound generation module.

3.3 Data acquisition protocol

To investigate the propagation of shear waves, a dedicated BM-mode scanning protocol was implemented in the OCT system. This acquisition scheme combines time-resolved measurements (M-mode) with lateral beam scanning (B-mode), enabling reconstruction of the spatiotemporal evolution of tissue displacement. Generally, the BM-mode protocol records a series of consecutive A-scans at each lateral position before moving the probing beam to the next measurement location (Fig. 7).

At each lateral position, the OCT probing beam remained stationary while a sequence of A-scans was acquired, forming an M-scan that captured the temporal evolution of the backscattered optical signal at different depths and at particular position of the beam. The acquisition was synchronized with the ultrasound excitation so that the transient mechanical response could be recorded. Once the M-scan acquisition was completed, the galvanometric scanning system moved the probing beam to the next lateral position, where the measurement procedure was repeated. By sequentially acquiring M-scans at multiple positions along the direction of elastic wave propagation, a spatially and temporally resolved dataset was obtained. Since the measurements at different lateral positions were performed sequentially, reconstruction of the propagating wavefront relied on the repeatability of the ultrasound excitation and precise synchronization between consecutive measurement sequences.

In the developed system, the swept-source laser operated at an A-scan rate of 200 kHz, corresponding to a temporal sampling interval of 5 µs. M-scan consisted of 1000 consecutive A-scans, providing a temporal observation window of 5 ms at each lateral position. The spatial sampling was determined by the scanning range and the number of measurement positions.

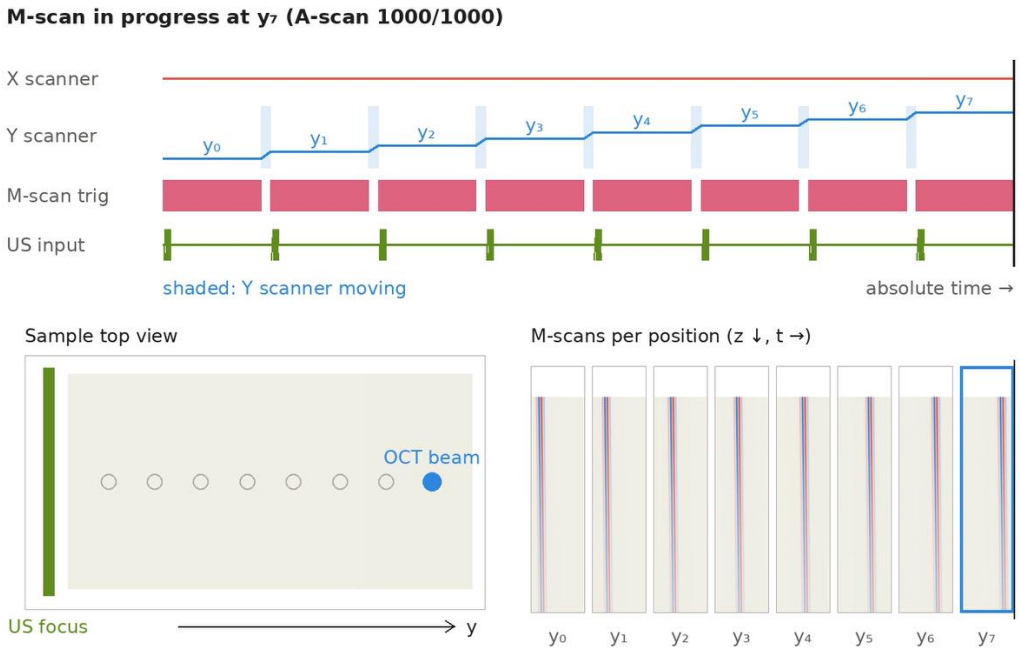

Figure 7. BM-mode acquisition protocol implemented for optical coherence elastography. The OCT probing beam is sequentially positioned at discrete lateral locations (y_0, y_1, …, y_7) along the direction of elastic wave propagation, while the X scanner remains stationary. At each lateral position, a series of consecutive A-scans is acquired to form an M-scan, providing depth-resolved information about tissue motion as a function of time. The ultrasound micro-tapping transducer is triggered at each measurement position to generate a repeatable mechanical excitation. Following completion of each M-scan, the Y scanner moves to the next lateral position, where the excitation and acquisition sequence is repeated. The ultrasound focal line is oriented perpendicular to the OCT scanning direction. Synchronization of the excitation and acquisition enables the individual M-scans to be combined into a three-dimensional dataset (y, z, t), from which spatiotemporal displacement maps can be reconstructed to characterize elastic wave propagation.

Consequently, the acquired dataset had three dimensions, corresponding to lateral position (x), imaging depth (z), and time (t). By extracting displacement profiles at a selected depth, or by tracking the displacement of the tissue surface, a two-dimensional spatiotemporal map, $\Delta z(y,t)$, could be reconstructed. Such maps enabled direct visualization of elastic wave propagation and provide the basis for further quantitative analysis, including the determination of wave propagation velocity, temporal attenuation, and frequency-dependent dispersion characteristics.

4 Results

4.1 OCE system with air-borne ultrasound stimulation

The experimental OCE system was developed by integrating the SS-OCT imaging platform with an ultrasound module for non-contact mechanical excitation of samples. The development process involved the assembly and alignment of the optical imaging subsystem, installation of the ultrasound transducer, integration of the excitation electronics, and implementation of synchronization between the ultrasound excitation and OCT data acquisition. Particular attention was given to the mechanical arrangement of the components to ensure precise positioning of the ultrasound focal region relative to the sample surface and the OCT probing beam. Accordingly, the ultrasound transducer was

mounted on an adjustable holder, allowing its position and orientation to be optimized while maintaining optical access to the investigated region. The system was configured to enable controlled excitation and phase-sensitive detection of propagating elastic waves using the dedicated BM-mode acquisition protocol. The integrated experimental platform was subsequently used for system diagnostics (measurements of the performance) and preliminary measurements on tissue-mimicking gelatin phantoms to evaluate its operation and establish measurement procedures. Figure 8 presents the photographs of the developed system, including the overall experimental arrangement and the configuration of the ultrasound transducer relative to the OCT scanning head and sample.

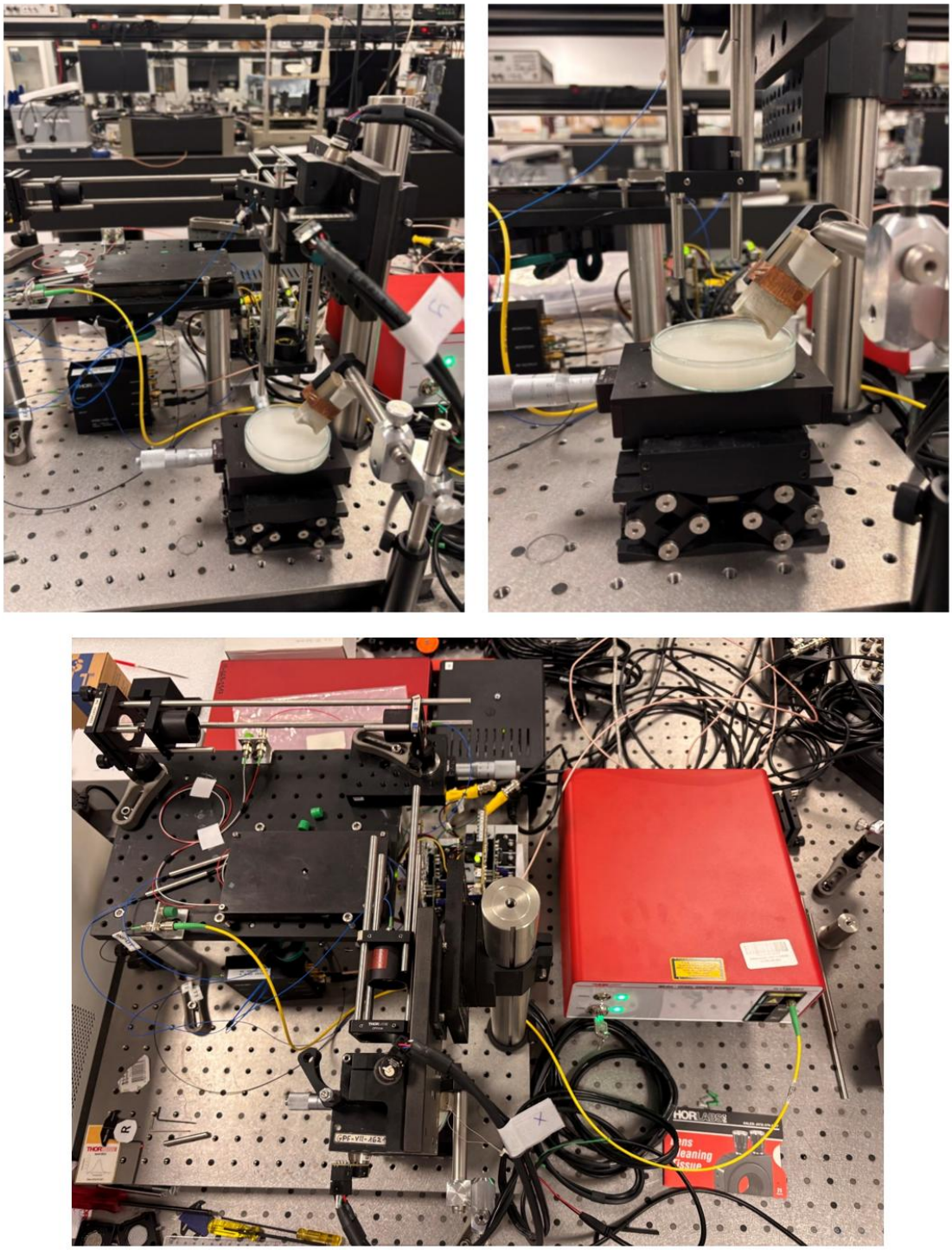

Figure 8. Experimental implementation of the developed optical coherence elastography system. Overview of imaging head of the integrated SS-OCT and acoustic micro-tapping experimental platform (top row, left). Close-up view of the air-coupled ultrasound transducer, OCT scanning head, and tissue-mimicking phantom, illustrating the spatial arrangement of the mechanical excitation and optical detection subsystems (top row, right). Top view of the entire interferometer (bottom row).

4.2 Performance of the system

The performance of the developed SS-OCT system was evaluated experimentally to determine its imaging capabilities and suitability for phase-sensitive optical coherence elastography. The characterization focused on five key parameters: axial imaging range, sensitivity roll-off, axial resolution, detection sensitivity, and phase stability.

We acquired a series of interferometric fringes for different optical path differences (OPD) by moving the reference arm mirror. The OPD difference between consecutive measurements was 0.3 mm. The measurements demonstrated a gradual decrease in the detected OCT signal with increasing depth, which is characteristic of SS-OCT systems (Fig. 9(a)). This behavior is associated primarily with the finite instantaneous linewidth of the swept laser, frequency bandwidth of the signal detection and acquisition.

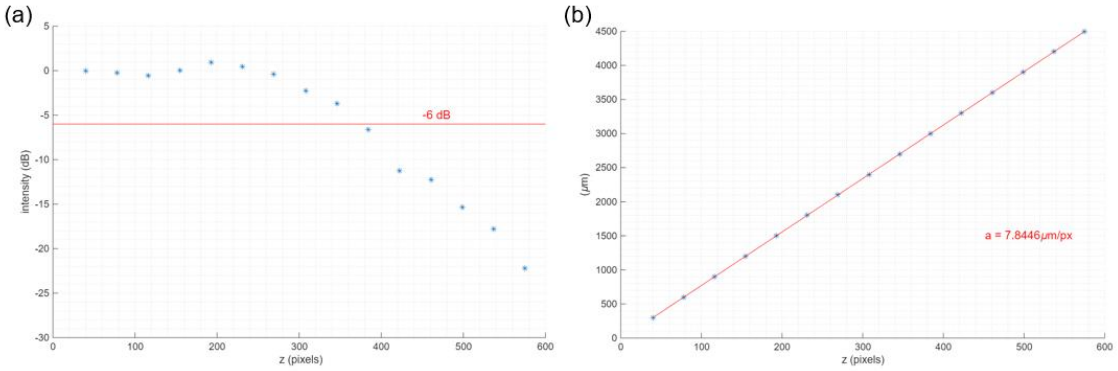

Figure 9. (a) Signal drop of the OCT system. (b) Calibration of the z-axis.

-6dB drop was observed at the depth corresponding to the bin #380. The plot in Fig. 9(b) shows how physical dimensions (z-axis) correspond to the bins obtained after Fourier transforming of the interferometric signal. The calibration factor of the depth is 7.8446 μm/bin. The experimentally determined axial imaging range was approximately 8 mm in air, while the signal attenuation reached −6 dB at a depth of 3 mm. The measured roll-off characteristics indicate the effective depth range over which the system maintains sufficient sensitivity for reliable detection of weakly backscattered optical signals. The obtained results show that with current detection, it is sufficient to image the cornea and the phantoms.

The axial resolution of the imaging system was determined experimentally from the axial point spread function (PSF) obtained using a mirror positioned in the sample arm. Figure 10 presents zoomed normalized PSF. In this case, 60x zero-padding was applied to the signal to better identify and measure the width of the PSF.

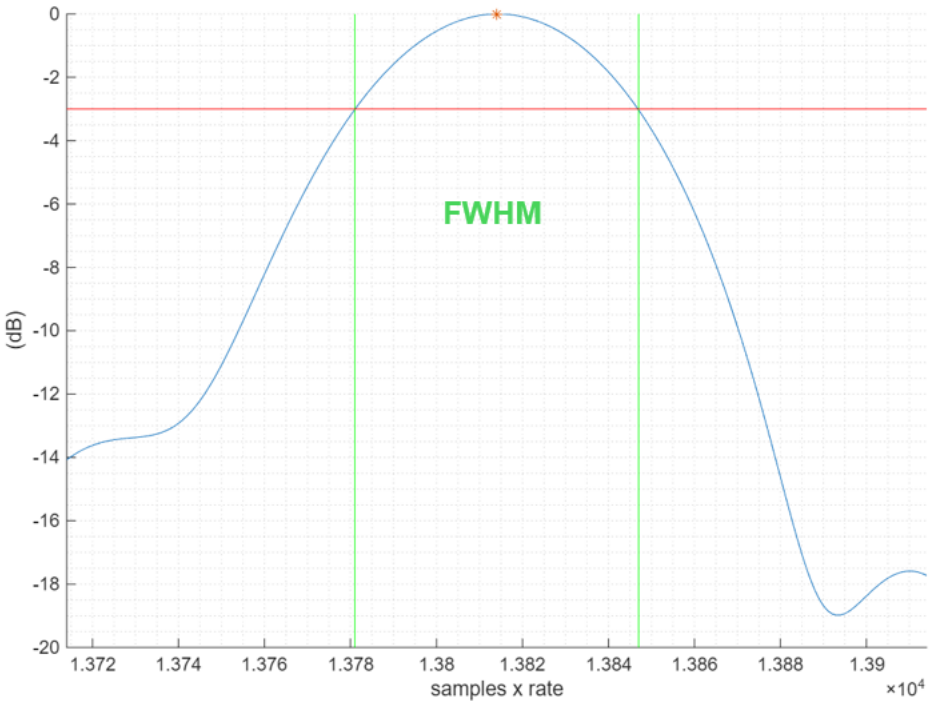

Figure 10. Experimentally measured axial point spread function of the SS-OCT system. The axial resolution was determined from the FWHM of the reconstructed reflection peak.

The measured full width at half maximum (FWHM) of the axial PSF was approximately 8.6 µm in air, corresponding to an axial resolution of approximately 6.4 µm in tissue, assuming a refractive index of 1.34. The experimentally measured axial resolution was compared with the theoretical axial resolution predicted from the spectral bandwidth of the laser source (7.45 µm). The experimentally obtained value was slightly lower than the theoretical prediction. Possible differences between theoretical and experimental values can be attributed to the non-Gaussian spectral characteristics of the swept source, wavelength characteristics of the fibers and data processing details.

The detection sensitivity of the SS-OCT system was evaluated by acquiring 1000 A-scans and measuring the signal-to-noise ratio (I_{peak}/σ_{noise}) of a calibrated reflection signal. The analysis was performed under controlled illumination conditions to determine the minimum sample reflectance detectable by the optical system. The power incident on the sample (mirror) was 4.38 mW. The resulted A-scan is demonstrated in Fig. 11.

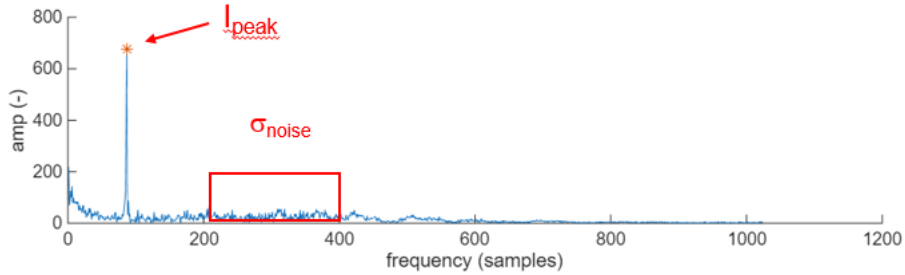

Figure 11. OCT reflection signal and background noise used for experimental determination of the detection sensitivity.

The experimentally determined maximum sensitivity was 99.13 dB, measured at a sample illumination power of 4.38 mW. The sensitivity was evaluated at the depth close to zero path delay.

The phase stability of the SS-OCT system was investigated to determine its ability to detect small axial displacements, which represents a critical requirement for optical coherence elastography. Measurements were performed using a stationary mirror positioned in the sample arm, with no external mechanical excitation applied. The temporal evolution of the differential OCT phase was analyzed over a sequence of consecutive A-scans. The measured standard deviation of the differential phase was approximately 5 mrad.

Transverse (lateral) scan calibration was performed to relate the voltage applied to scanners with the actual optical beam displacement in lateral direction. Concentric ring calibration phantom with periodicity of 1 mm was imaged with the system, and the spatial frequency of obtained pattern was measured (Fig. 12). The results showed that the calibration factor of 4.8 mm/V should be applied for the current lens objective.

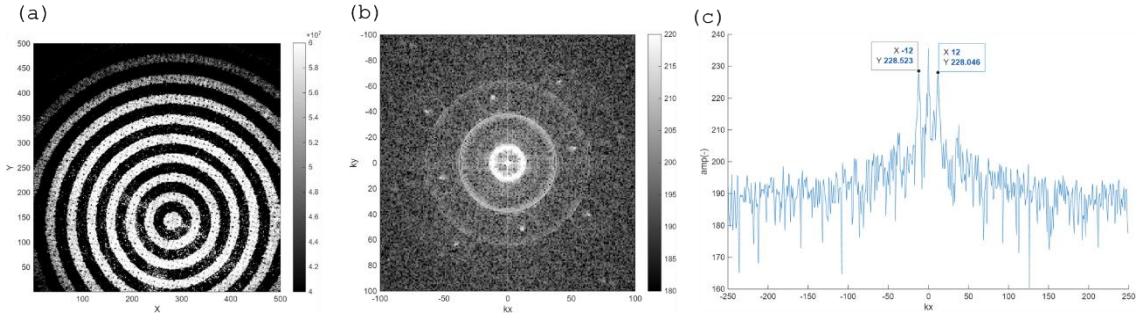

Figure 12. Calibration of transverse scanning. (a) En-face view of the acquired 3-D data set of the calibration phantom. (b) 2-D FFT of the projection. (c) Determination of the size of FFT ring is related to the spatial frequency of the ring pattern.

4.3 Visualization of shear wave propagation

To investigate the propagation of shear waves, gelatin phantoms with concentrations of 2% and 5% were prepared to mimic materials of increasing stiffness. he gelatin powder was dissolved in hot water under continuous, gentle stirring to obtain a homogeneous mixture while minimizing the formation of air bubbles. The solutions were subsequently transferred into circular glass containers with a diameter of approximately 80 mm and allowed to gel. The resulting phantoms had thicknesses ranging from approximately 8 mm. A small amount of titanium dioxide (TiO_2) was added to improve optical scattering and enhance the OCT signal from within the phantom volume, facilitating phase-sensitive measurements of internal mechanical displacements. The different gelatin concentrations were intended to provide samples exhibiting different mechanical responses to ultrasound excitation

The ability of the developed system to detect propagating elastic waves was investigated using gelatin phantoms with concentrations of 2% and 5%. The measurements were performed using the BM-mode acquisition protocol described in the previous section. The focused ultrasound transducer generated localized transient mechanical excitation at the phantom surface, while the phase-sensitive SS-OCT system recorded the resulting

mechanical displacements. At each lateral position, a sequence of 1000 consecutive A-scans was acquired to obtain the temporal evolution of the tissue response at different depths. The measurement was subsequently repeated at successive lateral positions along the direction of wave propagation. The resulting complex-valued OCT signals were used to extract phase variations associated with mechanically induced displacements. Figure 13 presents representative depth-resolved temporal measurements obtained for the 2% and 5% gelatin phantoms. The reconstructed M-scans reveal time-dependent phase variations associated with the mechanical response of the phantom following ultrasound excitation. The observed signals demonstrate that the developed OCT system is capable of detecting transient mechanical disturbances within the optically scattering material. Differences in the temporal evolution of the signals were observed between the investigated gelatin concentrations, reflecting differences in their mechanical response (Fig. 13).

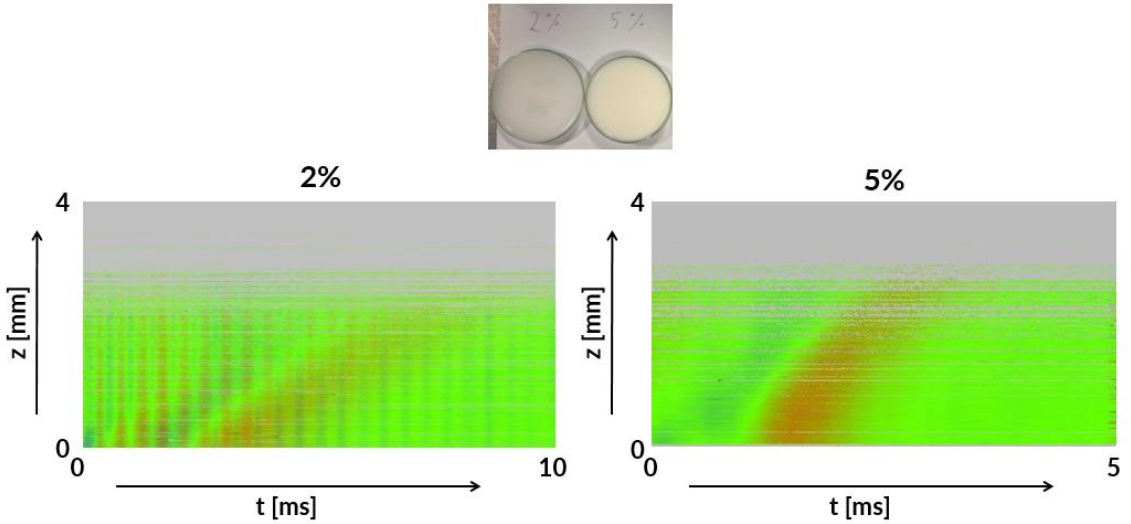

Figure 13. Photograph of gelatin phantoms prepared at concentrations of 2%, and 5% (top row). Phase-sensitive OCT detection of mechanically induced tissue displacements. Representative depth–time cross-sections (M-scans) obtained in 2% and 5% gelatin phantoms following ultrasound pulse excitation at the distance of 1.2 mm from the ultrasound focus. The temporal variation of the measured OCT signal demonstrates the transient mechanical response of the samples.

The reconstructed spatiotemporal displacement maps were used to estimate shear wave propagation velocity in the investigated phantoms. The velocity was determined from the relationship between the propagation distance and the temporal evolution of the observed wavefront. The analysis revealed a propagation velocity of approximately 0.51 m/s for the 2% gelatin phantom and 0.98 m/s for the 5% gelatin phantom (Fig. 14). The higher propagation velocity observed in the phantom with increased gelatin concentration is consistent with the expected increase in mechanical stiffness. The measured velocity in the 5% phantom was approximately 1.9 times higher than that in the 2% phantom.

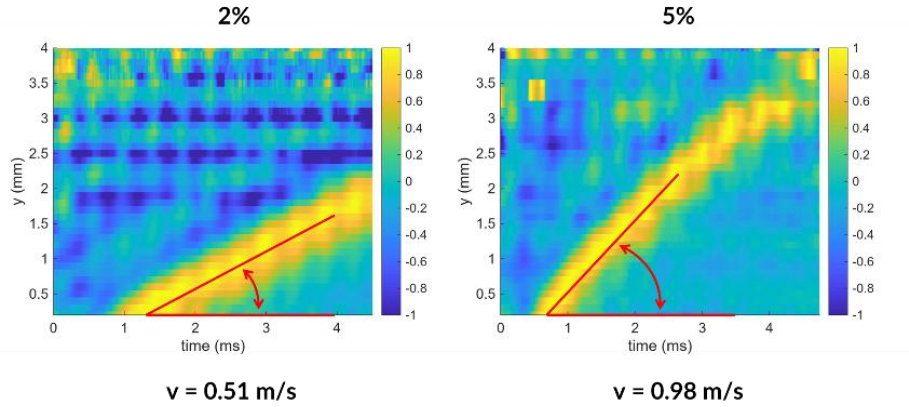

Figure 14. Spatiotemporal visualization of elastic wave propagation in gelatin phantoms. Displacement maps reconstructed from sequential M-scans acquired at different lateral positions. The propagating wavefront is identified by the inclined displacement band. The estimated propagation velocities were 0.51 m/s and 0.98 m/s for the 2% and 5% gelatin phantoms, respectively.

The experimental results demonstrate that the developed OCE platform is sensitive to differences in the mechanical properties of tissue-mimicking materials. The ability to discriminate between phantoms with different gelatin concentrations based on elastic wave propagation characteristics provides an initial validation of the measurement methodology and establishes a foundation for subsequent quantitative biomechanical characterization.

5 Summary & Conlusions

Within the framework of the BE-LIGHT project, a prototype TMV system integrating high-speed SS-OCT with non-contact ultrasound micro-tapping has been successfully developed and experimentally demonstrated. The developed instrument combines the advantages of optical interferometric detection with localized acoustic excitation, providing an experimental approach for investigating tissue biomechanical properties without direct mechanical contact.

The developed SS-OCT subsystem operates at a central wavelength of 1310 nm with an A-scan acquisition rate of 200 kHz. Experimental characterization demonstrated an axial imaging range of approximately 8 mm, a −6 dB sensitivity roll-off at 3 mm, an axial resolution of 8.6 µm in air, and a detection sensitivity of 99.1 dB. The measured phase stability of approximately 5 mrad indicates the capability of the optical system to detect subnanometer-scale axial displacement changes under controlled measurement conditions.

An important technological achievement was the successful integration of the air-coupled, cylindrically focused ultrasound transducer with the optical imaging system. The transducer enables localized, non-contact mechanical excitation through acoustic radiation force, while the dedicated electronic synchronization ensures a reproducible temporal relationship between ultrasound stimulation and OCT acquisition. Furthermore, a BM-mode acquisition protocol was implemented to record successive time-resolved M-scans at different lateral positions. This approach enables reconstruction of the spatiotemporal evolution of propagating elastic waves without requiring simultaneous acquisition of an entire OCT cross-section at ultrahigh frame rates.

The functionality of the integrated platform was demonstrated experimentally using tissue-mimicking gelatin phantoms with different mechanical properties. Phase-sensitive OCT measurements enabled visualization of ultrasound-induced elastic wave propagation and quantitative estimation of the corresponding propagation velocities. The measured velocities were approximately 0.51 m/s and 0.98 m/s for gelatin concentrations of 2% and 5%, respectively. The higher propagation velocity observed in the phantom with increased gelatin concentration is consistent with the expected increase in material stiffness. These results provide proof-of-concept evidence that the developed system can distinguish differences in the mechanical response of soft materials based on their elastic wave propagation characteristics.

Although the experimental results demonstrate the feasibility of the proposed approach, further development is required to establish quantitative measurements of intrinsic tissue mechanical properties. In particular, the interpretation of elastic wave propagation in thin and layered tissues requires consideration of sample geometry, boundary conditions, and frequency-dependent wave dispersion [6]. Future work will therefore focus on optimization of the excitation and acquisition protocols, validation of displacement and wave velocity measurements, and development of appropriate mechanical models for estimating tissue elasticity and viscoelasticity. Particular attention will be given to the application of the developed methodology to ex vivo corneal tissues [11], followed by investigations of its potential for in vivo ophthalmic measurements.

In conclusion, the objectives of developing and demonstrating a functional OCE prototype have been achieved. The integrated system enables non-contact mechanical excitation, phase-sensitive detection of transient tissue displacements, and visualization of propagating elastic waves. The experimental results establish the technological feasibility of the proposed methodology and provide a foundation for further research toward quantitative, spatially resolved assessment of corneal biomechanical properties and the development of novel optical biomarkers for ophthalmic diagnostics.

REFERENCES

[1] Piñero, D., & Alcón, N. (2015). Corneal biomechanics: A review. *Clinical and Experimental Optometry, 98*(2), 107–116. https://doi.org/10.1111/cxo.12230

[2] Elsheikh, A., Wang, D., Brown, M., Rama, P., Campanelli, M., & Pye, D. (2007). Assessment of corneal biomechanical properties and their variation with age. *Current Eye Research, 32*(1), 11–19. https://doi.org/10.1080/02713680601077145

[3] Ali, N., Patel, D., & McGhee, C. (2014). Biomechanical responses of healthy and keratoconic corneas measured using a noncontact Scheimpflug-based tonometer. *Investigative Ophthalmology & Visual Science, 55*(6), 3651–3659. https://doi.org/10.1167/iovs.13-13715

[4] Roberts, C., & Dupps, W. (2014). Biomechanics of corneal ectasia and biomechanical treatments. *Journal of Cataract & Refractive Surgery*, 40(6), 991–998. https://doi.org/10.1016/j.jcrs.2014.04.013

[5] Larin, K., & Sampson, D. (2017). Optical coherence elastography - OCT at work in tissue biomechanics. *Biomedical Optics Express, 8*(2), 1172–1202. https://doi.org/10.1364/BOE.8.001172

[6] Zvietcovich, F., & Larin, K. (2022). Wave-based optical coherence elastography: The 10-year perspective. *Progress in Biomedical Engineering, 4*(1), 012007. https://doi.org/10.1088/2516-1091/ac4512

[7] Garra, B. (2015). Elastography: History, principles, and technique comparison. *Abdominal Imaging, 40*(4), 680–697. https://doi.org/10.1007/s00261-014-0305-8

[8] Dorronsoro, C., Pascual, D., Pérez-Merino, P., Kling, S., & Marcos, S. (2012). Dynamic OCT measurement of corneal deformation by an air puff in normal and cross-linked corneas. *Biomedical Optics Express, 3*(3), 473–487. https://doi.org/10.1364/BOE.3.000473

[9] Alonso-Caneiro, D., Karnowski, K., Kaluzny, B., Kowalczyk, A., & Wojtkowski, M. (2011). Assessment of corneal dynamics with high-speed swept source optical coherence tomography combined with an air puff system. *Optics Express, 19*(15), 14188–14199. https://doi.org/10.1364/OE.19.014188

[10] Ambroziński, Ł., Song, S., Yoon, S. et al. (2016). Acoustic micro-tapping for non-contact 4D imaging of tissue elasticity. *Scientific Reports, 6*, 38967. https://doi.org/10.1038/srep38967

[11] Kirby, M., Pelivanov, I., Regnault, G., Pitre, J., Wallace, R., O'Donnell, M., Wang, R., & Shen, T. (2023). Acoustic micro-tapping optical coherence elastography to quantify corneal collagen cross-linking: An ex vivo human study. *Ophthalmology Science, 3*(2), 100257. https://doi.org/10.1016/j.xops.2022.100257